
UNCERTAINTY-GUIDED CROSS ATTENTION ENSEMBLE MEAN TEACHER FOR SEMI-SUPERVISED MEDICAL IMAGE SEGMENTATION

Meghana Karri

Machine and Hybrid Intelligence Lab
Northwestern University
Chicago, USA
meghana.karri@northwestern.edu

Amit Soni Arya

School of Computer Science Engineering and Technology
Bennett University
India
amitsoniuoh@gmail.com

Koushik Biswas

Machine and Hybrid Intelligence Lab
Northwestern University
Chicago, USA
koushik.biswas@northwestern.edu

Nicolo Gennaro

Northwestern University
Chicago, USA
nicolo.gennaro@northwestern.edu

Vedat Cicek, Gorkem Durak, Yury Velichko, Ulas Bagci

Machine and Hybrid Intelligence Lab
Northwestern University
Chicago, USA
{vedat.cicek, gorkem.durak, y-velichko, ulas.bagci}@northwestern.edu

ABSTRACT

This work proposes a novel framework, Uncertainty-Guided Cross Attention Ensemble Mean Teacher (UG-CENT), for achieving state-of-the-art performance in semi-supervised medical image segmentation. UG-CENT leverages the strengths of co-training and knowledge distillation by combining a Cross-attention Ensemble Mean Teacher framework (CENT) inspired by Vision Transformers (ViT) with uncertainty-guided consistency regularization and Sharpness-Aware Minimization emphasizing uncertainty. UG-CENT improves semi-supervised performance while maintaining a consistent network architecture and task setting by fostering high disparity between sub-networks. Experiments demonstrate significant advantages over existing methods like Mean Teacher and Cross-pseudo Supervision in terms of disparity, domain generalization, and medical image segmentation performance. UG-CENT achieves state-of-the-art results on multi-center prostate MRI and cardiac MRI datasets, where object segmentation is particularly challenging. Our results show that using only 10% labeled data, UG-CENT approaches the performance of fully supervised methods, demonstrating its effectiveness in exploiting unlabeled data for robust medical image segmentation. The code is publicly available at <https://github.com/Meghna13/UG-CENT>

1 Introduction

Medical image segmentation, essential for accurate diagnosis and treatment, has significantly benefited from recent advancements in deep learning, achieving higher accuracy and automation Chen et al. [2018], Ronneberger et al. [2015]. However, training these models requires a large amount of labeled data, a laborious process requiring expert knowledge and prone to human error and bias. As a result, labeled data is often limited to well-studied structures like major organs or common cancers, while unlabeled data is readily available and less expensive to acquire. This has motivated the exploration of semi-supervised learning (SSL) techniques Van Engelen and Hoos [2020]. SSL

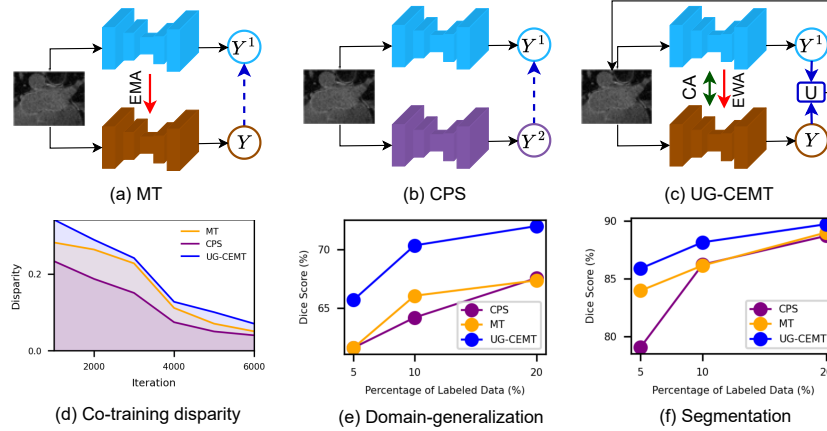


Figure 1: Comparison of architectures and their performance for SSL segmentation tasks: (a) Mean Teacher (MT), (b) Cross-Pseudo supervision (CPS), (c) UG-CEMT framework (proposed), (d) disparity between co-training sub-networks w.r.t Jaccard metric, (e) domain generalization effectiveness for multi-site prostate dataset, and (f) segmentation performance on single-site LA dataset.

leverages both abundant unlabeled data and limited labeled data, enhancing model generalizability, reducing annotation burden, and unlocking the power of unlabeled data for various medical imaging tasks, including anomaly detection, disease segmentation, and classification Berthelot et al. [2019], Cascante-Bonilla et al. [2021], Luo et al. [2018], Yang et al. [2021]. However, despite its potential, SSL for medical imaging faces several key challenges: data quality and mislabels, limited control over large-scale unlabeled data, bias due to data selection, explainability issues, and domain generalization problems. Following these challenges, various SSL methods have been proposed, with consistency regularization Tarvainen and Valpola [2017], Xie et al. [2020] and pseudo-labeling Lee et al. [2013], Yao et al. [2022], Shen et al. [2023] are the two mainstream SSL approaches used for medical image segmentation. In this study, we propose an alternative method combining the complementary strengths of these two primary approaches via cross-supervision and knowledge distillation (i.e., Teacher-Student sub-networks). Specifically, we propose an *Uncertainty-Guided Cross Attention Ensemble Mean Teacher (UG-CEMT)* framework, which excels at maintaining higher disparity between co-training segmentation sub-networks by leveraging high-confidence predictions. This, in turn, enhances semi-supervised segmentation performance while using a consistent backbone network and task settings. Unlike traditional approaches that rely heavily on pseudo generation, our UG-CEMT framework prioritizes consistency regularization, which enforces the model to maintain consistent predictions across different perturbations of the same input data. This focus on consistency over prediction generation helps to reduce the propagation of errors that can occur when low-confidence predictions are used during training. For instance, while standard mean teacher frameworks like UA-MT Yu et al. [2019a] primarily utilize a static approach to uncertainty estimation, UG-CEMT dynamically adapts its learning process through a novel cross-attention mechanism and two-step training process, ensuring robust feature alignment and improving generalization. Moreover, unlike approaches such as MCF-Net Wang et al. [2023], which may employ pseudo-labels without considering uncertainty, UG-CEMT leverages uncertainty-guided consistency using the Monte Carlo dropout (MC Dropout) to prioritize high-confidence predictions, significantly enhancing segmentation performance. Additionally, Sharpness-Aware Minimization (SAM) regularization further enhances the model’s generalization by smoothing the loss landscape and incorporating uncertainty to improve robustness. Figure 1 illustrates high-level comparisons of architectures and their performance for SSL segmentation tasks: mean teacher (MT) Tarvainen and Valpola [2017], cross-pseudo supervision (CPS) Chen et al. [2021], and our proposed method UG-CEMT. Disparity between co-training networks, effectiveness of these methods on domain generalization, and medical image segmentation are also illustrated. In the experiments, we show detailed results supporting our observations and findings.

Summary of our contributions are as follows:

- We identify and address critical limitations in existing co-training-based semi-supervised segmentation approaches, specifically the inadequate disparity among sub-networks and reliance on low-confidence predictions. UG-CEMT introduces a novel cross-attention mechanism that dynamically enhances disparity and an uncertainty-guided consistency strategy that prioritizes high-confidence predictions, collectively leading to superior segmentation performance.

- Our framework’s two-step training process, driven by uncertainty estimation, not only improves the initial training phase but also guides the model in refining its predictions in the subsequent phase. This process, combined with SAM regularization, ensures that the model remains robust across different domains and data variations.
- Comprehensive experiments across various public medical image segmentation datasets, including challenging 3D scenarios, validate the novel integration of cross-attention and uncertainty-guided regularization in UG-CEMT. Our results demonstrate the clear superiority of UG-CEMT over existing state-of-the-art approaches, particularly in maintaining network disparity and enhancing domain generalization.

Clinical significance of the problem: This study addresses two critical tasks: cardiac MRI and prostate MRI analysis. Cardiac MRI is vital for diagnosing and monitoring cardiovascular diseases, the leading cause of mortality worldwide. Accurate left atrium (LA) segmentation is key for evaluating cardiac conditions like atrial fibrillation Mortazi et al. [2023], but is challenging due to size, shape variations, and inconsistent image quality. Prostate cancer, the most diagnosed cancer in men and the fifth leading cause of cancer deaths globally Belue et al. [2024], also relies on MRI for detection and staging. Segmentation is difficult due to the similar density of surrounding tissues and variability in image quality across centers. Our work uses multi-center prostate MRI data to assess the generalization of the proposed SSL system.

2 Related Work

The objective of SSL is to enhance the effectiveness of supervised learning (SL) by utilizing unlabeled data in conjunction with labeled data Van Engelen and Hoos [2020]. A prevalent method in SSL is the inclusion of a regularization factor in the SL objective function, which enables the model to capitalize on unlabeled data. In this regard, SSL algorithms can be broadly classified into two primary approaches: *consistency regularization* Tarvainen and Valpola [2017] and *pseudo-labeling* Lee et al. [2013]. Pseudo-labeling attempts to generate pseudo-labels for unlabeled data, mimicking ground truth labels used in supervised training. Consistency regularization, on the other hand, enforces the model’s predictions to remain consistent across different input variations. Both of these techniques have been successfully applied to SSL for image classification, achieving exceptional results Sohn et al. [2020], Zhang et al. [2021].

Challenges of SSL: Many SSL methods leverage labeled data supervision not just for initialization or training convergence, but as a crucial element to explicitly guide knowledge extraction from unlabeled data Miyato et al. [2018]. This is particularly relevant in the context of predominantly labeled clinical datasets, where foreground features such as appearance, shape, and texture are often consistent across diverse samples. By bridging the gap between labeled and unlabeled data within the entire training set, SSL has the potential to effectively transfer prior knowledge from labeled examples to unlabeled data, overcoming the performance limitations often encountered in SSL approaches.

Co-teaching methods: Recent approaches in SSL utilize mutual learning or co-teaching paradigms to achieve promising results Yu et al. [2019b], Chen et al. [2021]. These methods combine consistency regularization with entropy minimization. They employ two models that are trained simultaneously, with each model predicting the output of its counterpart. This approach has shown significant improvement in segmentation performance for semi-supervised medical image segmentation, as demonstrated by MC-Net Seibold et al. [2022].

Consistency regularization: Consistency regularization, exemplified by MT Tarvainen and Valpola [2017], enforces consistent predictions across perturbed inputs for a student-teacher network pair via gradient descent and an exponential weighted average (EWA), respectively. Subsequent methods have built on this idea. For example, Luo et al. [2018] introduced a graph-based method to ensure adjacent points remain consistent under perturbations. Miyato et al. Miyato et al. [2018] incorporated adversarial perturbations into consistency learning, leading to interpolation-consistent training (ICT) Verma et al. [2022] to avoid potential generalization issues. Wang et al. Wang et al. [2021] combined multitask learning with MT, using triple uncertainty to guide the student model. Huang et al. Huang et al. [2022] proposed a method for neuron segmentation based on pixel-level prediction consistency. However, these methods often overlook the interactions between sub-networks and may struggle to address inherent network biases. *Our proposed UG-CEMT framework addresses these limitations by employing a cross-attention mechanism to enhance feature alignment and information exchange between student and teacher models.*

Problem of low-confidence pseudo labels: While consistency regularization is an effective SSL method, current co-training models using consistency regularization often converge rapidly to a consensus, leading to low-confidence pseudo labels from perturbed input data during training. This premature convergence results in the model degenerating into self-training. Maintaining disparity among sub-networks is essential for effective co-training, as it ensures that the information provided by each sub-network remains complementary. Furthermore, the effectiveness of these models is substantially influenced by the quality of pseudo labels, which should exhibit low uncertainty.

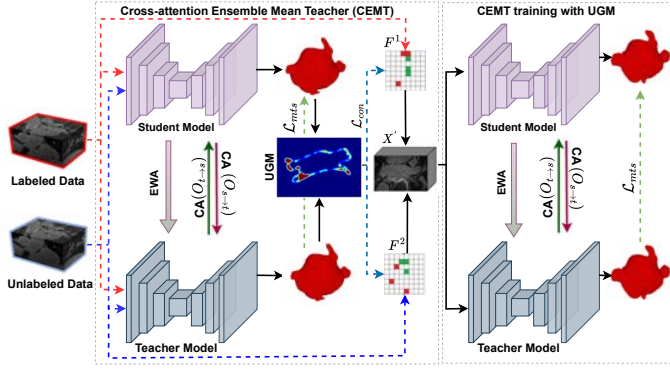


Figure 2: The proposed UG-CENT architecture. UG-CENT creates new samples X' from input data using UGM. Cross-Attention (CA) is applied between the student and teacher model, where $O_{(s \rightarrow t)}$ and $O_{(t \rightarrow s)}$ represent outputs of attention mechanism from student to teacher, and teacher to student respectively.

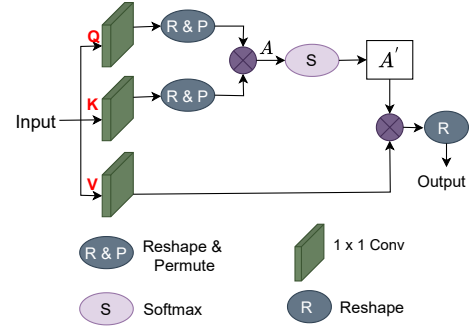


Figure 3: Overview of the proposed cross-attention (CA) mechanism (inspired by ViT).

Uncertainty-guided semi-supervised learning: Exploiting model uncertainty (epistemic) for consistency regularization offers promise in SSL. However, accurate estimation and effective utilization remain challenges. Common methods rely on MC Dropout Gal and Ghahramani [2016] or prediction variance Zhang et al. [2021]. Prior works leverage uncertainty for loss reweighting Yu et al. [2019a] or contrastive sample selection Wang et al. [2022]. These methods often require a fixed threshold for filtering low-confidence pseudo-labels, a process hampered by the difficulty of setting an appropriate value. Our UG-CENT framework addresses this by estimating uncertainty via MC Dropout and entropy calculation. Instead of filtering pseudo-labels, we integrate this uncertainty into consistency regularization, enabling the model to learn robustly from both labeled and unlabeled data based on dynamic confidence levels. This eliminates the need for fixed thresholds, ultimately improving segmentation performance.

3 Methods

Our proposed UG-CENT framework addresses critical challenges in existing co-training-based semi-supervised segmentation methods by enhancing model disparity among sub-networks, leveraging a cross-attention mechanism, an uncertainty-guided consistency regularization process, and SAM regularization. These components collectively ensure that our model effectively utilizes both labeled and unlabeled data for superior segmentation performance. As illustrated in Figure 2, the proposed model includes a two-step training phase. In the first step, we train the CEMT using both labeled and unlabeled data to generate uncertainty-guided maps. In the CEMT framework, the uncertainty-guided map ensures low uncertainty for high-confidence predictions. In the second step, we retrain the CEMT model using these uncertainty-guided maps to further enhance segmentation performance.

3.1 Cross-attention (CA) mechanism

As shown in Figure 3, the cross-attention mechanism in our UG-CENT framework is designed to robustly align features and facilitate information exchange between the student and teacher models, thereby enhancing overall segmentation performance. For the student model's feature map X_s and the teacher model's feature map X_t , we first project these features into queries (Q), keys (K), and values (V) via learnable weight matrices W_Q, W_K, W_V as: $Q_s = X_s W_Q^s$, $K_t = X_t W_K^t$, $V_t = X_t W_V^t$, $Q_t = X_t W_Q^t$, $K_s = X_s W_K^s$, $V_s = X_s W_V^s$. The cross-attention from the student model to the teacher model is then computed by taking the dot product of the student queries Q_s and the teacher keys K_t , scaling by the square root of the key dimension $\sqrt{d_k}$, and applying a softmax function to obtain the attention weights. These weights are then used to compute a weighted sum of the teacher values V_t :

$$CA_{s \rightarrow t}(Q_s, K_t, V_t) = \text{Softmax} \left(\frac{Q_s K_t^T}{\sqrt{d_k}} \right). \quad (1)$$

Similarly, the cross-attention (CA) from the teacher model to the student model is computed as:

$$CA_{t \rightarrow s}(Q_t, K_s, V_s) = \text{Softmax} \left(\frac{Q_t K_s^T}{\sqrt{d_k}} \right). \quad (2)$$

These attention weights are used to compute a weighted sum of the values:

$$O_{s \rightarrow t} = CA_{s \rightarrow t}(Q_s, K_t, V_t)V_t, \quad (3)$$

$$O_{t \rightarrow s} = CA_{s \rightarrow t}(Q_t, K_s, V_s)V_s. \quad (4)$$

The output of the attention mechanism is combined with the original feature maps using another learnable parameter γ : $X'_s = \gamma \dot{O}_{s \rightarrow t} + X_s$, and $X'_t = \gamma \dot{O}_{t \rightarrow s} + X_t$. The updated features X'_s and X'_t are then used in subsequent layers of the student and teacher models, respectively.

3.2 Semi-supervised segmentation

Assuming a training set with N labeled and M unlabeled examples. Let the labeled dataset be denoted as $\mathcal{D}_L = \{(a_i, b_i)\}_{i=1}^M$, and the unlabeled dataset be represented as $\mathcal{D}_U = \{a_i\}_{i=M+1}^{M+N}$. Here $a_i \in \mathbb{R}^{H \times W \times D}$ refers to the input image (volume), and $b_i \in \{0, 1\}^{H \times W \times D}$ indicates the corresponding ground-truth annotation (i.e., segmentation maps). The primary objective of our semi-supervised segmentation framework is to minimize a combined loss function that integrates both supervised and unsupervised components:

$$\min_{\theta} \left(\sum_{i=1}^M \mathcal{L}_s [f(a_i; \theta), b_i] + \lambda \sum_{j=M+1}^{M+N} \mathcal{L}_c [f(a_j; \theta, \zeta), f(a_j; \theta, \zeta')] \right) \quad (5)$$

Where \mathcal{L}_s represents the supervised loss, such as cross-entropy loss, which evaluates the accuracy of the network's output against the labeled data. \mathcal{L}_c indicates the unsupervised consistency loss, which quantifies the agreement between the predictions of the student and teacher sub-networks for the same input a_j under different perturbations. The segmentation network is denoted by $f(\cdot)$, and (θ, ζ) , (θ, ζ') pair represent the model and perturbations (e.g., input noise and dropout) parameters applied to the teacher and student sub-networks, respectively. The term λ indicates a ramp-up coefficient that balances the supervised and unsupervised loss components.

3.3 Uncertainty-guided consistency regularization

The Uncertainty-Guided Consistency Regularization framework leverages the concept of uncertainty to enhance the robustness and reliability of the semi-supervised learning process. This framework estimates model uncertainty and integrates it with the mean teacher model to improve the training of the student model.

1) Uncertainty estimation: While various techniques exist for estimating uncertainty in deep learning models, we opt for MC Dropout due to its several advantages. MC Dropout offers a well-established and computationally efficient approach, allowing us to leverage the existing network architecture without introducing significant modifications. Additionally, MC Dropout provides inherent interpretability by directly reflecting the model's confidence in its predictions. This interpretability is crucial in our setting, where understanding and prioritizing high-confidence predictions for uncertainty-guided consistency regularization is essential Isler et al. [2023]. Herein, we employ MC dropout during training by performing multiple stochastic forward passes with dropout to generate a set of predictions for each input. The uncertainty is then quantified using the entropy of these predictions. For an input x , we obtain N stochastic predictions $\{\hat{y}_1, \hat{y}_2, \dots, \hat{y}_N\}$ by applying dropout: $\hat{y}_{mean} = \frac{1}{N} \sum_{i=1}^N \hat{y}_i$. The entropy of the mean prediction is calculated to quantify the uncertainty:

$$Entropy(\hat{y}_{mean}) = - \sum_c \hat{y}_{mean}^c \log(\hat{y}_{mean}^c), \quad (6)$$

where c denotes the class index. Higher entropy indicates greater uncertainty in the prediction.

2) Ensemble mean teacher model: Recent research has demonstrated that ensemble mean teacher predictions from different training stages can enhance prediction quality. By leveraging these ensembled predictions as the teacher's predictions, we can achieve improved segmentation results. Consequently, the teacher model's weights θ_t are updated using an exponential weighted average (EWA) of the student model's weights θ . This EWA approach ensures that the teacher model captures information from different stages of the training process. The update rule for the teacher model's weights at training step t is given by: $\theta_t = \beta \theta_{t-1} + (1 - \beta) \theta_t$, where β is the EWA decay rate controlling the update pace.

3) Consistency regularization with uncertainty guidance: Consistency regularization encourages the student model to produce similar predictions under different perturbations. In the UG-CENT framework, this regularization is guided

by the estimated uncertainty. Specifically, we focus on areas with low uncertainty to enforce consistency, as these areas are more likely to provide reliable supervision signals. The consistency loss \mathcal{L}_{cons} is defined as:

$$\mathcal{L}_{cons} = \mathbb{E}_{x \sim u} \left[U(x) \left\| f_s(x) - f_t(x') \right\|_2^2 \right], \quad (7)$$

where U represents the distribution of unlabeled data, x' is a perturbed version of x , and $U(x)$ is the uncertainty weight based on the entropy: $U(x) = \exp(-Entropy(\hat{y}_{mean}))$. This weighting ensures that regions with lower uncertainty have a higher impact on the consistency loss, encouraging the model to learn from more reliable predictions.

3.4 Overall training objective

We utilize V-Net Milletari et al. [2016] as our backbone network and modify it by removing the short residual connections in each convolution block. Our training objective combines dice and cross-entropy loss. To enable V-Net for uncertainty estimation, dropout layers with a dropout rate of 0.5 are added after both the R-Stage 1 and L-stage 5 layers. Dropout is activated during training and uncertainty estimation but deactivated during testing. We set the EWA decay parameter α to 0.99, consistent with previous research. A time-dependent Gaussian warming-up function $\phi(t) = 0.1 \times e^{(-5(1 - \frac{t}{t_{max}})^2)}$ is used to balance the supervised and unsupervised consistency losses, where t is the current training step and t_{max} is the maximum training step Li et al. [2020], Wu et al. [2021]. This approach ensures that the supervised loss term dominates at the start, preventing the network from becoming stuck in a degenerate solution with no meaningful target predictions for unlabeled data. For uncertainty estimation, we set $T = 8$ to balance the quality of uncertainty estimation with training efficiency. As training progresses, this method allows the student model to gradually learn from increasingly uncertain cases. To further enhance generalization and robustness, we incorporate the SAM optimizer Wu et al. [2024]. SAM optimizes the model weights by not only minimizing the training loss but also ensuring the loss landscape is smooth (by acting as a regularizer). This is achieved by performing a gradient ascent step followed by a gradient descent step, effectively flattening the minima in the loss surface. The SAM optimizer requires careful tuning of its parameters, such as the radius of the neighborhood ρ , which we empirically set to achieve a balance between performance and stability. For our implementation, we use a SAM optimizer with $\rho = 0.5$.

4 Experiments and Results

Datasets: We evaluate our model on two challenging medical image segmentation datasets. First, publicly available *LA-Dataset* (3D Left Atrium Segmentation challenge) Xiong et al. [2021] comprises 100 3D (volumetric) gadolinium-enhanced MRI scans (GE-MRIs) with corresponding left atrium (LA) labels for training and validation. All images were cropped to center on the heart location and normalized. We split the data into 80 images for training and 20 for testing by following challenge guidelines. Second, *Multi-Site Prostate MRI Segmentation* dataset Liu et al. [2020] is designed to assess model robustness by containing T2-weighted MRI scans from six different medical centers (multi-site) with distinct data distributions. This dataset includes data from NCI-ISBI 2013, I2CVB, and PROMISE12 datasets, further separated by acquisition site. In total, there are 116 image volumes: 30 cases from each of RUNMC and BMC sites, 30 from NCI-ISBI2013’s HCRUDB19 site, and 13, 12, and 12 cases from UCL, BIDME, and HK sites within PROMISE12, respectively. We split the data into 92 images for training and 24 for testing by following the challenge guidelines.

Evaluation metrics: We use four performance measures to assess our model’s effectiveness, including edge sensitive metrics: Average Surface Distance (ASD) and 95% Hausdorff Distance (95HD), and regional sensitive metrics: Jaccard similarity coefficient (Jaccard) and Dice similarity coefficient (Dice).

Implementation details: With PyTorch library and A6000 NVIDIA GPU, we augmented the training data with random cropping to sub-volumes of size $112 \times 112 \times 80$. The training process utilizes the SAM optimizer with a base learning rate of 0.01, momentum of 0.9, weight decay of 0.0001, and a neighborhood size parameter $\rho = 0.05$. We used a batch size of 4 with an equal distribution of labeled and unlabeled images. Our implementation includes a comprehensive set of parameters to manage consistency regularization effectively. We set λ_s to 0.05 for balancing similarity loss and use a consistency ramp-up period of 40 epochs. The temperature for sharpening is set to 0.1. We use a memory bank with 256 embeddings per class, each embedding having a dimension of 64. Additionally, we filter 12,800 unlabeled embeddings to calculate. During training, we log the loss values and learning rate using TensorBoard and save the model checkpoints at regular intervals. The model is trained for a maximum of 6000 iterations, with the learning rate reduced by 0.1 every 2500 iterations.

Performance evaluation on LA dataset: We compared UG-CEM with the state-of-the-art SSL methods including UA-MT Yu et al. [2019a], which leverages an uncertainty-guided approach; MC-Net Wu et al. [2021], which utilizes mutual consistency learning with cycle pseudo-labels; DTC Luo et al. [2021], which introduces multi-task consistency for medical image segmentation; SASSNet Li et al. [2020], which incorporates geometric constraints into the network;

Table 1: Comparison of the proposed UG-CEMT with other state-of-the-art SSL methods on LA dataset for 6000 iterations.

Method	(% of images used)		Metrics			
	Labeled	Unlabeled	Dice \uparrow	Jaccard \uparrow	95HD \downarrow	ASD \downarrow
B-VNet	80(100%)	0	91.20	83.05	4.56	1.95
V-VNet	80(100%)	0	90.96	82.89	5.00	1.72
B-VNet	16(20%)	0	84.26	73.54	18.12	4.95
V-VNet	16(20%)	0	83.11	72.47	14.77	3.82
UA-MT	4(5%)	76	78.23	65.03	22.17	8.63
DTC	4(5%)	76	80.16	67.88	21.45	7.18
CPS	4(5%)	76	79.07	68.26	16.23	6.89
SASSNet	4(5%)	76	80.21	67.01	21.64	7.20
MC-Net	4(5%)	76	80.92	68.25	17.25	3.43
MT	4(5%)	76	83.97	72.67	15.56	5.03
CEMT(Ours)	4(5%)	76	85.23	75.16	5.12	1.32
UG-CEMT(Ours)	4(5%)	76	85.89	76.23	3.39	0.69
UA-MT	8(10%)	72	85.81	75.41	18.25	5.04
DTC	8(10%)	72	84.55	73.91	13.80	3.69
CPS	8(10%)	72	86.23	76.22	11.68	3.65
SASSNet	8(10%)	72	85.71	75.13	14.60	4.00
MC-Net	8(10%)	72	85.13	77.49	10.35	1.85
MT	8(10%)	72	86.15	76.16	11.37	3.60
CEMT(Ours)	8(10%)	72	87.03	78.26	3.39	0.67
UG-CEMT(Ours)	8(10%)	72	88.16	79.83	3.08	0.51
UA-MT	16(20%)	64	88.13	78.04	9.66	2.62
DTC	16(20%)	64	87.79	78.60	10.29	2.50
CPS	16(20%)	64	88.72	80.10	7.49	1.91
SASSNet	16(20%)	64	87.86	77.79	12.31	3.27
MC-Net	16(20%)	64	89.18	79.94	6.52	1.66
MT	16(20%)	64	89.01	81.21	6.08	1.96
CEMT(Ours)	16(20%)	64	89.12	80.94	3.78	0.66
UG-CEMT(Ours)	16(20%)	64	89.73	81.63	2.20	0.50

CPS Chen et al. [2021] which uses cross pseudo supervision approach. Additionally, we implemented MT-based UA-MT for a more comprehensive comparison Tarvainen and Valpola [2017]. The results are presented in Table 1. We evaluated our model on different (%) of labeled data, including 5%, 10%, and 20%. We also reported the performance of V-VNet (Vanilla-VNet) and B-VNet (Bayesian-VNet) by increasing the dropout at 100% and 20% labeled data to serve as reference upper bounds and baselines. As shown in Table 1, all SSL methods benefit from incorporating unlabeled data. UA-MT outperformed the MT, indicating that the uncertainty map can enhance the student model’s performance. Among the comparison methods, MC-Net demonstrated the best results in terms of Dice and Jaccard with stable performance for 20% labeled data. Overall, CPS excelled in 95HD and ASD metrics compared to all existing methods, and SSANet performed well, suggesting that incorporating shape priors can enhance edge segmentation. The proposed UG-CEMT framework outperformed all state-of-the-art methods across all metrics and also substantially improved results on edge-sensitive metrics such as 95HD and ASD were obtained. Compared to SASSNet, UG-CEMT reduced 95HD from 12.31 to 2.30 mm and ASD from 3.27 to 0.50 mm for 20% labeled data, and a similar range of decrement was there for 10% and 5% labeled data, indicating a more stable and accurate performance.

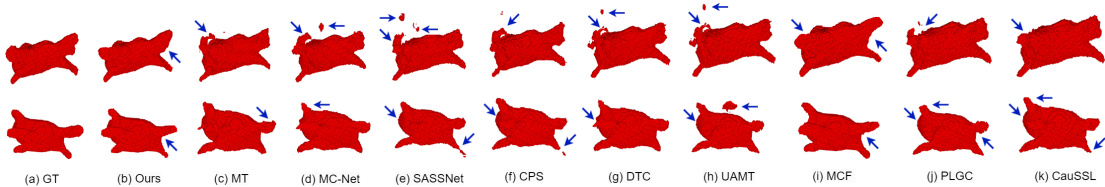


Figure 4: Visualization of 3D segmentation outcomes of various SSL methods for 20% labeled data on LA dataset.

Performance evaluation on multi-site prostate dataset: Prostate segmentation is challenging due to small and variable organ shape, scanner, and other physiological variations as well as the domain generalization issues that arise from multi-source datasets. As illustrated in Table 2, we provided the results at different (%) of labeled images. Like LA segmentation, B-VNet outperforms V-VNet in a fully supervised manner. UA-MT outperforms all the other existing methods, such as dice and Jaccard. Notably, the performance of these existing approaches on the two datasets is inconsistent; it shows which method performs worse in LA segmentation and describes an advantage on the multi-site prostate datasets, such as UA-MT, DTC, and SSANet. The gap between LA and prostate segmentation performance is

Table 2: Comparison of the proposed UG-CEMT with other state-of-the-art methods on multi-site prostate dataset for 6000 iterations.

Method	(%) of images used		Metrics	
	labeled	unlabeled	Dice \uparrow	Jaccard \uparrow
V-VNet	92(100%)	0	78.76	66.52
B-VNet	92(100%)	0	80.76	67.49
V-VNet	18(20%)	0	64.63	54.87
B-VNet	18(20%)	0	66.55	53.56
UA-MT	5(5%)	87	62.16	52.58
DTC	5(5%)	87	60.23	51.68
CPS	5(5%)	87	61.58	53.36
SASSNet	5(5%)	87	62.89	52.18
MC-Net	5(5%)	87	61.34	51.23
MT	5(5%)	87	61.57	51.78
CEMT(Ours)	5(5%)	87	63.68	55.82
UG-CEMT(Ours)	5(5%)	87	65.68	56.87
UA-MT	9(10%)	83	65.67	57.13
DTC	9(10%)	83	65.23	57.86
CPS	9(10%)	83	64.17	56.15
SASSNet	9(10%)	83	65.01	57.39
MC-Net	9(10%)	83	64.23	56.69
MT	9(10%)	83	66.04	56.52
CEMT(Ours)	9(10%)	83	69.23	59.26
UG-CEMT(Ours)	9(10%)	83	70.36	60.73
UA-MT	18(20%)	74	68.43	59.68
DTC	18(20%)	74	68.01	59.00
CPS	18(20%)	74	67.56	58.86
SASSNet	18(20%)	74	67.33	58.18
MC-Net	18(20%)	74	67.89	58.67
MT	18(20%)	74	67.36	57.24
CEMT(Ours)	18(20%)	74	70.13	60.16
UG-CEMT(Ours)	18(20%)	74	72.02	61.29

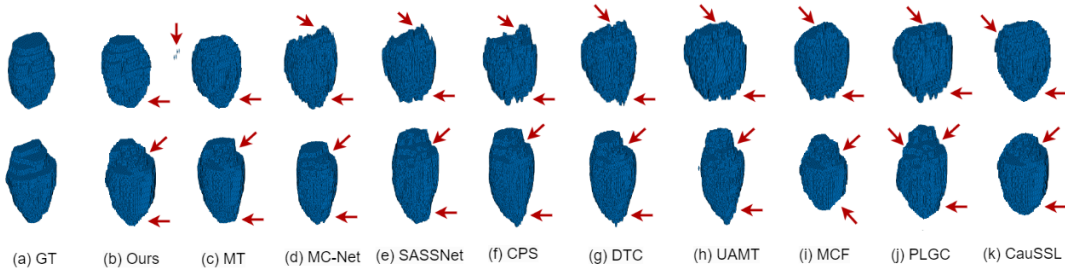


Figure 5: Visualization of 3D segmentation outcomes of various SSL methods for 20% labeled data on multi-site prostate dataset.

more because of the complexity of multi-source data. Our proposed method consistently showed better results, on the other hand.

Qualitative analysis: Figures 4 and 5 display some of the LA and prostate segmentation results. As shown, CPS and SASSNet on LA segmentation, and MC-Net and CPS on prostate segmentation, tend to under-segment specific regions, likely due to restricted generalization abilities. MCF-Net Wang et al. [2023], PSGC Basak and Yin [2023], and CauSSL Miao et al. [2023] show comparable performance with our model. In contrast, our UG-CEMT framework produces more precise outcomes, capturing finer segmentation features with a more effective training strategy. Our model generates relatively high-confidence predictions from the UGM images. Initially, UG-CEMT produces high uncertainty guided maps (For additional visual results, please refer to the *supplementary material* Figure 1), but

progressively enhances its confidence in the input images during training. These results demonstrate that UGM can enable SSL approaches to produce high-confidence predictions, ensuring more effective co-training with UG-CENT. Additionally, we conducted additional experiments using a pancreas CT dataset Roth et al. [2015] to further assess the generalizability of UG-CENT across different imaging modalities. The qualitative and quantitative results of these experiments, along with detailed dataset descriptions and analysis, can be found in the *supplementary material*.

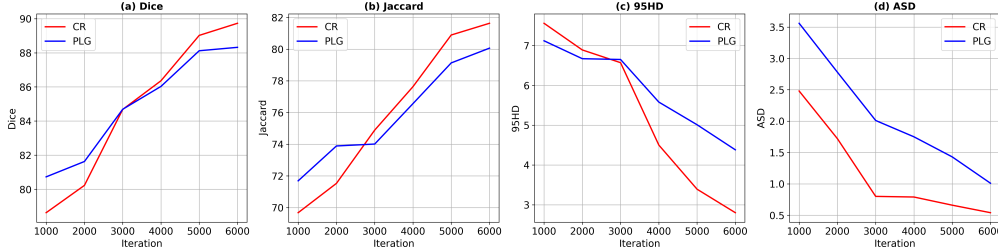


Figure 6: Performance comparison between pseudo label generation (PLG) and consistency regularization (CR) label training

Table 3: Performance comparison when different regularization techniques used during training on LA dataset.

Regularizer	Dice \uparrow	Jaccard \uparrow	95HD \downarrow	ASD \downarrow
L1	88.02	79.96	6.08	2.16
L2	88.34	79.82	5.76	3.68
SAM	89.73	81.63	2.8	0.5

Table 4: Ablation study for combining different components on LA dataset. ST: student-teacher, CA: cross-attention, EWA: exponential weighted average, U: uncertainty guided map.

labeled data	Study	ST	CA	EWA	U	Dice \uparrow	95HD \downarrow
5%	Baseline	✓				78.16	11.89
	MT	✓		✓		83.72	6.37
	CEMT	✓	✓	✓		85.23	5.12
	UG-CENT	✓	✓	✓	✓	85.89	3.39
10%	Baseline	✓				84.13	9.15
	MT	✓		✓		86.28	5.78
	CEMT	✓	✓	✓		87.03	3.39
	UG-CENT	✓	✓	✓	✓	88.16	3.08
20%	Baseline	✓				85.17	7.18
	MT	✓		✓		87.89	4.68
	CEMT	✓	✓	✓		89.02	3.78
	UG-CENT	✓	✓	✓	✓	89.73	2.20

Computational cost analysis: The proposed UG-CENT model consists of 9.66M parameters and requires 47.1G MACs (FLOPs) for a single forward pass. Despite the complexity introduced by the cross-attention mechanism, the model achieves significant performance improvements while remaining computationally feasible. The total training time of ≈ 1 hour 50 minutes for 6000 iterations, demonstrates the model’s efficiency and suitability for real-world deployment. A detailed analysis is provided in the *supplementary material*.

4.1 Ablation study

We conducted ablation experiments to demonstrate the effectiveness of each component in our UG-CENT framework including regularization methods.

Effect of regularization techniques: We examined the impact of different regularization techniques on the performance of our UG-CENT framework on LA dataset for 20% labeled images for 6000 iterations. As shown in Table 3, we compared L1 and L2 regularization with SAM. Using L1 regularization, the model achieved a Dice score of 88.02% and a 95HD of 6.08 mm. L2 regularization slightly improved the performance, with a Dice score of 88.34% and a 95HD of 5.76 mm. However, SAM significantly outperformed both L1 and L2 methods, achieving the highest Dice score of 89.73% and the lowest 95HD of 2.8 mm. These results demonstrate that SAM effectively enhances model generalization and performance, making it a superior regularization technique for our framework.

Effects of different components: As shown in Table 4, we conducted ablation experiments to demonstrate the effectiveness of each component in our UG-CENT framework for 6000 iterations. The baseline ST setup achieved

a Dice score of 78.16% and a 95HD of 11.59 mm with 5% labeled data. Adding EWA improved performance to a Dice score of 83.72% and a 95HD of 6.37 mm. Incorporating CA further enhanced performance, achieving a Dice score of 85.23% and a 95HD of 5.12 mm. The complete UG-CENT framework, integrating all components, achieved the highest Dice score of 85.89% and the lowest 95HD of 3.39 mm with 5% labeled data. This demonstrates that each component contributes to overall performance improvement, with the full model yielding the best results (For qualitative results, please refer to the *supplementary material* Figure 2).

CR and PLG: To understand dynamic performance changes during training, we compared consistency regularization (CR) with pseudo label generation (PLG) in our UG-CENT framework. Figure 6 shows performance metrics over iterations for Dice, Jaccard, 95HD, and ASD on the LA dataset with 20% labeled images. Initially, PLG outperformed CR within the first 2,000 iterations. However, beyond 2,000 iterations, CR surpassed PLG, indicating its effectiveness in maintaining high performance as training progresses. After 5,000 iterations, the gap widened, with CR demonstrating superior performance across all metrics, highlighting its robustness in leveraging unlabeled data for consistent performance improvement.

5 Discussion and Concluding Remarks

In this work, we presented UG-CENT, a novel framework for semi-supervised medical image segmentation that leverages uncertainty-guided cross-attention ensemble mean teacher learning. Our experiments on challenging 3D left atrium and multi-site prostate MRI datasets demonstrate that UG-CENT outperforms state-of-the-art SSL methods across various metrics and labeled data ratios. The superior performance of UG-CENT can be attributed to several key factors including (1) enhanced feature alignment, (2) uncertainty-guided learning, and (3) improved generalization. Our ablation studies reveal the importance of each component in the UG-CENT framework. The combination of cross-attention, exponential weighted average, and uncertainty-guided maps consistently yields the best performance across different labeled data ratios. The comparison between consistency regularization (CR) and pseudo-label generation (PLG) highlights the long-term stability and effectiveness of CR in leveraging unlabeled data. This finding suggests that carefully designed consistency constraints can be more beneficial than relying solely on generated pseudo-labels, especially as training progresses. The UG-CENT makes it particularly suitable for clinical applications, where obtaining large labeled datasets is challenging due to the need for expert annotations. By leveraging a combination of labeled and unlabeled data, UG-CENT reduces annotation costs while maintaining high performance, which is critical in real-world medical imaging workflows. While UG-CENT shows promising results, there are limitations and areas for future work. *Computational complexity:* The cross-attention mechanism and uncertainty estimation increase computational overhead. Future work could explore more efficient implementations or lightweight alternatives. *Generalization to other tasks:* While we focused on left atrium and prostate segmentation, further studies could investigate the applicability of UG-CENT to a broader range of medical imaging tasks and modalities. *Uncertainty calibration:* Although our method leverages uncertainty estimates, further research into calibrating these uncertainties could potentially lead to even more reliable predictions.

Acknowledgments This study is supported by NIH grants: R01-CA246704, R01 CA240639, R01-HL171376, and U01-CA268808.

References

- Liang-Chieh Chen, Yukun Zhu, George Papandreou, Florian Schroff, and Hartwig Adam. Encoder-decoder with atrous separable convolution for semantic image segmentation. In *Proceedings of the European conference on computer vision (ECCV)*, pages 801–818, 2018.
- Olaf Ronneberger, Philipp Fischer, and Thomas Brox. U-net: Convolutional networks for biomedical image segmentation. In *Medical image computing and computer-assisted intervention—MICCAI 2015: 18th international conference, Munich, Germany, October 5-9, 2015, proceedings, part III 18*, pages 234–241. Springer, 2015.
- Jesper E Van Engelen and Holger H Hoos. A survey on semi-supervised learning. *Machine learning*, 109(2):373–440, 2020.
- David Berthelot, Nicholas Carlini, Ian Goodfellow, Nicolas Papernot, Avital Oliver, and Colin A Raffel. Mixmatch: A holistic approach to semi-supervised learning. *Advances in neural information processing systems*, 32, 2019.
- Paola Cascante-Bonilla, Fuwen Tan, Yanjun Qi, and Vicente Ordonez. Curriculum labeling: Revisiting pseudo-labeling for semi-supervised learning. In *Proceedings of the AAAI conference on artificial intelligence*, volume 35, pages 6912–6920, 2021.
- Yucen Luo, Jun Zhu, Mengxi Li, Yong Ren, and Bo Zhang. Smooth neighbors on teacher graphs for semi-supervised learning. In *Proceedings of the IEEE conference on computer vision and pattern recognition*, pages 8896–8905, 2018.

- Ceyuan Yang, Zhirong Wu, Bolei Zhou, and Stephen Lin. Instance localization for self-supervised detection pretraining. In *Proceedings of the IEEE/CVF Conference on Computer Vision and Pattern Recognition*, pages 3987–3996, 2021.
- Antti Tarvainen and Harri Valpola. Mean teachers are better role models: Weight-averaged consistency targets improve semi-supervised deep learning results. *Advances in neural information processing systems*, 30, 2017.
- Qizhe Xie, Zihang Dai, Eduard Hovy, Thang Luong, and Quoc Le. Unsupervised data augmentation for consistency training. *Advances in neural information processing systems*, 33:6256–6268, 2020.
- Dong-Hyun Lee et al. Pseudo-label: The simple and efficient semi-supervised learning method for deep neural networks. In *Workshop on challenges in representation learning, ICML*, volume 3, page 896. Atlanta, 2013.
- Huifeng Yao, Xiaowei Hu, and Xiaomeng Li. Enhancing pseudo label quality for semi-supervised domain-generalized medical image segmentation. In *Proceedings of the AAAI conference on artificial intelligence*, volume 36, pages 3099–3107, 2022.
- Zhiqiang Shen, Peng Cao, Hua Yang, Xiaoli Liu, Jinzhu Yang, and Osmar R Zaiane. Co-training with high-confidence pseudo labels for semi-supervised medical image segmentation. *arXiv preprint arXiv:2301.04465*, 2023.
- Lequan Yu, Shujun Wang, Xiaomeng Li, Chi-Wing Fu, and Pheng-Ann Heng. Uncertainty-aware self-ensembling model for semi-supervised 3d left atrium segmentation. In *Medical image computing and computer assisted intervention—MICCAI 2019: 22nd international conference, Shenzhen, China, October 13–17, 2019, proceedings, part II 22*, pages 605–613. Springer, 2019a.
- Yongchao Wang, Bin Xiao, Xiuli Bi, Weisheng Li, and Xinbo Gao. Mcf: Mutual correction framework for semi-supervised medical image segmentation. In *Proceedings of the IEEE/CVF conference on computer vision and pattern recognition*, pages 15651–15660, 2023.
- Xiaokang Chen, Yuhui Yuan, Gang Zeng, and Jingdong Wang. Semi-supervised semantic segmentation with cross pseudo supervision. In *Proceedings of the IEEE/CVF conference on computer vision and pattern recognition*, pages 2613–2622, 2021.
- Aliasghar Mortazi, Vedat Cicek, Elif Keles, and Ulas Bagci. Selecting the best optimizers for deep learning-based medical image segmentation. *Frontiers in Radiology*, 3:1175473, 2023.
- Mason J Belue, Stephanie A Harmon, Dong Yang, Julie Y An, Sonia Gaur, Yan Mee Law, Evrim Turkbey, Ziyue Xu, Jesse Tetreault, Nathan S Lay, et al. Deep learning-based detection and classification of bone lesions on staging computed tomography in prostate cancer: A development study. *Academic radiology*, 2024.
- Kihyuk Sohn, David Berthelot, Nicholas Carlini, Zizhao Zhang, Han Zhang, Colin A Raffel, Ekin Dogus Cubuk, Alexey Kurakin, and Chun-Liang Li. Fixmatch: Simplifying semi-supervised learning with consistency and confidence. *Advances in neural information processing systems*, 33:596–608, 2020.
- Bowen Zhang, Yidong Wang, Wenxin Hou, Hao Wu, Jindong Wang, Manabu Okumura, and Takahiro Shinozaki. Flexmatch: Boosting semi-supervised learning with curriculum pseudo labeling. *Advances in Neural Information Processing Systems*, 34:18408–18419, 2021.
- Takeru Miyato, Shin-ichi Maeda, Masanori Koyama, and Shin Ishii. Virtual adversarial training: a regularization method for supervised and semi-supervised learning. *IEEE transactions on pattern analysis and machine intelligence*, 41(8):1979–1993, 2018.
- Xingrui Yu, Bo Han, Jiangchao Yao, Gang Niu, Ivor Tsang, and Masashi Sugiyama. How does disagreement help generalization against label corruption? In *International conference on machine learning*, pages 7164–7173. PMLR, 2019b.
- Constantin Marc Seibold, Simon Reiß, Jens Kleesiek, and Rainer Stiefelhagen. Reference-guided pseudo-label generation for medical semantic segmentation. In *Proceedings of the AAAI conference on artificial intelligence*, volume 36, pages 2171–2179, 2022.
- Vikas Verma, Kenji Kawaguchi, Alex Lamb, Juho Kannala, Arno Solin, Yoshua Bengio, and David Lopez-Paz. Interpolation consistency training for semi-supervised learning. *Neural Networks*, 145:90–106, 2022.
- Kaiping Wang, Bo Zhan, Chen Zu, Xi Wu, Jiliu Zhou, Luping Zhou, and Yan Wang. Triple-uncertainty guided mean teacher model for semi-supervised medical image segmentation. In *Medical Image Computing and Computer Assisted Intervention—MICCAI 2021: 24th International Conference, Strasbourg, France, September 27–October 1, 2021, Proceedings, Part II 24*, pages 450–460. Springer, 2021.
- Wei Huang, Chang Chen, Zhiwei Xiong, Yueyi Zhang, Xuejin Chen, Xiaoyan Sun, and Feng Wu. Semi-supervised neuron segmentation via reinforced consistency learning. *IEEE Transactions on Medical Imaging*, 41(11):3016–3028, 2022.

- Yarin Gal and Zoubin Ghahramani. Dropout as a bayesian approximation: Representing model uncertainty in deep learning. In *international conference on machine learning*, pages 1050–1059. PMLR, 2016.
- Kaiping Wang, Bo Zhan, Chen Zu, Xi Wu, Jiliu Zhou, Luping Zhou, and Yan Wang. Semi-supervised medical image segmentation via a tripled-uncertainty guided mean teacher model with contrastive learning. *Medical Image Analysis*, 79:102447, 2022.
- Ilkin Isler, Debesh Jha, Curtis Lisle, Justin Rineer, Patrick Kelly, Bulent Aydogan, Mohamed Abazeed, Damla Turgut, and Ulas Bagci. Self-supervised learning for organs at risk and tumor segmentation with uncertainty quantification. In *2023 3rd International Conference on Electrical, Computer, Communications and Mechatronics Engineering (ICECCME)*, pages 1–6. IEEE, 2023.
- Fausto Milletari, Nassir Navab, and Seyed-Ahmad Ahmadi. V-net: Fully convolutional neural networks for volumetric medical image segmentation. In *2016 fourth international conference on 3D vision (3DV)*, pages 565–571. Ieee, 2016.
- Shuailin Li, Chuyu Zhang, and Xuming He. Shape-aware semi-supervised 3d semantic segmentation for medical images. In *Medical Image Computing and Computer Assisted Intervention–MICCAI 2020: 23rd International Conference, Lima, Peru, October 4–8, 2020, Proceedings, Part I 23*, pages 552–561. Springer, 2020.
- Yicheng Wu, Minfeng Xu, Zongyuan Ge, Jianfei Cai, and Lei Zhang. Semi-supervised left atrium segmentation with mutual consistency training. In *Medical image computing and computer assisted intervention–MICCAI 2021: 24th international conference, Strasbourg, France, September 27–October 1, 2021, proceedings, part II 24*, pages 297–306. Springer, 2021.
- Tao Wu, Tie Luo, and Donald C Wunsch II. Cr-sam: Curvature regularized sharpness-aware minimization. In *Proceedings of the AAAI Conference on Artificial Intelligence*, volume 38, pages 6144–6152, 2024.
- Zhaohan Xiong, Qing Xia, Zhiqiang Hu, Ning Huang, Cheng Bian, Yefeng Zheng, Sulaiman Vesal, Nishant Ravikumar, Andreas Maier, Xin Yang, et al. A global benchmark of algorithms for segmenting the left atrium from late gadolinium-enhanced cardiac magnetic resonance imaging. *Medical image analysis*, 67:101832, 2021.
- Quande Liu, Qi Dou, Lequan Yu, and Pheng Ann Heng. Ms-net: Multi-site network for improving prostate segmentation with heterogeneous mri data. *IEEE Transactions on Medical Imaging*, 2020.
- Xiangde Luo, Jieneng Chen, Tao Song, and Guotai Wang. Semi-supervised medical image segmentation through dual-task consistency. In *Proceedings of the AAAI conference on artificial intelligence*, volume 35, pages 8801–8809, 2021.
- Hritam Basak and Zhaozheng Yin. Pseudo-label guided contrastive learning for semi-supervised medical image segmentation. In *Proceedings of the IEEE/CVF conference on computer vision and pattern recognition*, pages 19786–19797, 2023.
- Juzheng Miao, Cheng Chen, Furui Liu, Hao Wei, and Pheng-Ann Heng. Caussl: Causality-inspired semi-supervised learning for medical image segmentation. In *Proceedings of the IEEE/CVF International Conference on Computer Vision*, pages 21426–21437, 2023.
- Holger R Roth, Le Lu, Amal Farag, Hoo-Chang Shin, Jiamin Liu, Evrim B Turkbey, and Ronald M Summers. Deeporgan: Multi-level deep convolutional networks for automated pancreas segmentation. In *Medical Image Computing and Computer-Assisted Intervention–MICCAI 2015: 18th International Conference, Munich, Germany, October 5-9, 2015, Proceedings, Part I 18*, pages 556–564. Springer, 2015.